**M.S. DISSERTATION**

# Colorimeteric Plasmonic Gas Sensor

**By**

**Jason J. Kim**

**August 2019**

**SEOUL NATIONAL UNIVERSITY**

**COLLEGE OF ENGINEERING**

**DEPARTMENT OF MATERIALS SCIENCE AND ENGINEERING**

# Colorimeteric Plasmonic Gas Sensor

Advisor: Prof. Ho Won Jang

by

Jason J. Kim

A thesis submitted to the Graduate Faculty of Seoul National University in partial fulfillment of the requirements for the Degree of Master

Department of Materials Science and Engineering

August 2019

Approved

by

Chairman of Advisory Committee: Sang Bum Kim (인)

Vice-chairman of Advisory Committee: Ho Won Jang (인)

Advisory Committee: Soo Young Kim (인)

## Abstract

# Colormetric Plasmonic Gas Sensor

Jason J. Kim

Department of Materials Science and Engineering

Graduate School

Seoul National University

The field of plasmonics has been of much interest over the past few decades, showing potential for use in various applications. Of these applications, the use of plasmonics in gas sensing is currently being investigated. In order to enhance the sensitivity, selectivity, and durability of gas sensors, many studies have focused on the use of plasmonics as optical sensors for gas sensing. Because optical sensors require no contact measurements, are electromagnetically noise independent, and do not require a heating mechanism they can be more reliable compared to electrical sensors.

In this study, the concept of optical interference coupled with the electromagnetic enhancement of plasmon resonances is used to design a sensor for the colorimetric detection of gases. The localized surface plasmon resonance (LSPR) and surface plasmon polariton (SPP) caused by the interaction of light with the plasmonic layer

of the sensor is utilized in fabricating sensors of various structural colors. The structural colors were simulated through Lumerical software Finite Difference Time Domain (FDTD) Solutions then fabricated for comparison.

The resonances that occur at the plasmonic layers of the sensors are extremely sensitive to changes in its environment. Therefore, nanostructured metal oxides decorated with noble metals as catalysts were used as the dielectric medium for the adsorption and desorption of gases. The adsorption of gas is expected to bring about a change in the sensors' optical properties, which in turn causes a peak shift in the scattering, absorption, and transmission spectra. These peak shifts and the possible color change associated with these shifts are used as the response for our plasmonic sensor.

**Keywords:** Tungsten oxide, Metal oxide nanostructure, Optical sensor, Localized surface plasmon resonance, Optical interference, Noble metal nanoparticle

**Student Number: 2017-22001**

Jason J. Kim

# Table of Contents

**Chapter 5. Summary**

## List of Tables

## List of Figures

# Chapter 1.

# Introduction

## 1.1 Background

For the past few decades, environmental pollutions have drastically increased, degrading the quality of life for humans globally. Of the various pollutions, air pollution caused mostly by the burning of fossil fuels in businesses, factories, and transportations have a major impact on human health as well as the environment in the form of acid rain, climate change, and many others. Therefore, the monitoring of these harmful gas emissions has become increasingly important. There are many efforts in the development of gas sensors for this reason.

Most conventional sensors today are chemoresistive sensors that utilize metal oxide semiconductors (MOS) as the sensing material. In the 1960s, changes in the conductivity due to the adsorption or desorption of gases on the surface of metal oxides was demonstrated.[1] This phenomenon was further improved and utilized in many chemiresistive sensors used today. The change in resistance that occurs with adsorption of reducing or oxidizing gases is used as a response for these type of sensors. However, one significant drawback of these type of sensors is that it requires high operating temperature, which increases power consumption which, in turn, reduces sensor lifetime.[2] Although there are many studies which seek to ameliorate these flaws through nanostructuring and noble metal decoration[3–7], many efforts are also being made to develop sensors with the advantages of chemoresistive sensors such

as high response, selectivity, and cost effective but are more power efficient, durable, and miniscule. For this reason, over the last decade, many studies have been carried out to develop plasmon-based sensors.

Following the success of the surface-enhanced Raman spectroscopy, plasmonics has attracted much attention for its potential in many different applications. With the advances in nanostructure fabrication in both “top-down” methods such as electron-beam and “bottom-up” techniques such as nanosphere lithography, plasmonic resonances became controllable allowing them to be applied to gas sensing.[8] The concept of plasmonic sensing rely on the ability of metal particles to concentrate light into deep subwavelength volumes. This is caused by the interaction between the particles and the electromagnetic component of light which induces collective oscillations of the conduction electrons of the particles against the restoring force of the nuclei.[8] When these particles become smaller than the wavelength of light, they form a localized oscillation called Localized Surface Plasmon Resonance (LSPR) whereas on a thin film surface, they form a Surface Plasmon Resonance (SPR).[8] Fig.1 illustrates the interaction between light and the interfaces of metallic surfaces which exhibit plasmon resonance. These plasmonic resonances are extremely sensitive to its environment. Therefore, the plasmonic resonances and their response to changes in their environment is utilized as the main mechanism behind plasmonic gas sensors.

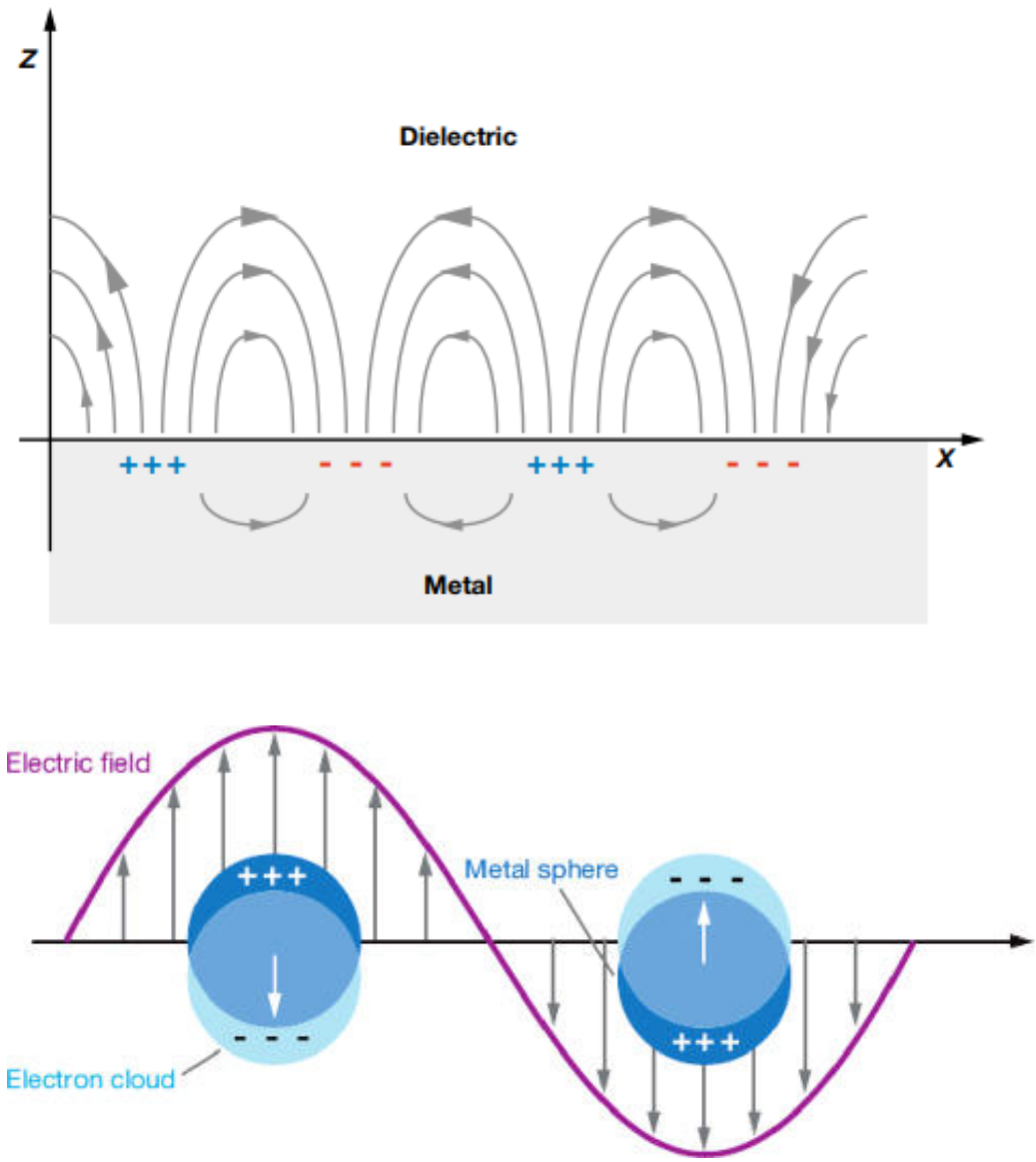


**Figure 1.1** Schematic of illustrating (a) Surface plasmon polariton (propagating plasmon) and (b) Localized surface plasmon resonance (LSPR). Figure from Ref. 8.

## 1.2 Objectives of this study

For this study, plasmonics and the concept of optical interference were utilized to develop a colorimetric plasmonic gas sensor. When two light waves are superimposed, they create either constructive or destructive interference, leading to interference fringes. When these interference fringes occur on thin structured layers, they provide vibrant colors called structural colors. The optical interferences mainly depend of the thickness, periodic patterns, and refractive index of the film, factors which can be controlled.

Since the optical interferences result from the superimposition of light, the constructive interference provides the maximum intensity of light which would greatly enhance the plasmonic effect.[9] By applying these concepts, a 3D nanostructure was fabricated which consisted of three main layers: plasmonic top layer, sensing middle layer, and mirror bottom layer. The optical behavior of the reflected light was controlled by coupling the plasmonic layer with the optical interferences. For the sensing layer, tungsten trioxide ($WO_3$) was deposited through electron beam evaporator for the detection of $H_2$ and $NO_2$. By controlling the thickness of the $WO_3$ layer, various structural colors can be produced. The $WO_3$ was annealed for crystallization of the film, as the e-beam deposited $WO_3$ is in an amorphous state, which does not adsorb gases efficiently.

As mentioned previously, the optical interferences mainly depend on the

thickness, periodic patterns, and the refractive index of the film. Therefore, the main mechanism behind this colorimetric plasmonic gas sensor is in the change in refractive index of the sensing material with the adsorption of gases which, in turn, causes a change in the optical interference, thus a shift in the plasmonic resonance peak. Consequently, the plasmonic sensors presented in this thesis were studied systematically using various experiments including Ultraviolet-visible spectrography, scanning electron microscopy (SEM), and finite-difference time domain (FDTD) simulations.

In Chapter 3, optical interference based plasmonic sensors utilizing $WO_3$ thin films with Au plasmonic layer on Al mirror layer for the detection of $NO_2$ are presented. With Au deposition on $WO_3$ thin films, the electric fields at the interfaces between the Au nanoparticles and $WO_3$ thin films are drastically enhanced with illumination. By varying the thicknesses of the $WO_3$ films, the distance between the Au plasmonic layer and the reflecting mirror layer can be controlled. This allows us to control the structural colors of the sensors, therefore create a color palette accordingly. With exposure to $NO_2$, the sensors showed a slight blue-shift in their scattering spectra which can be correlated to the shift in the plasmon resonance peak.

In Chapter 4, hydrogen detecting optical interference based plasmonic sensor was fabricated. The sensor consisted of a Au plasmonic layer on Pd decorated $WO_3$ nanorod on Al mirror layer. Resembling the thin film sensor,

this nanostructured sensor utilized the optical interference fringes that occurs with the reflection of light off the mirror layer to construct structural colors. However, unlike the thin film, this nanostructured sensor was decorated with Pd nanoparticles which are known for its affinity to $H_2$.[10,11] The $WO_3$ provides larger active surface area while the Pd readily adsorbs $H_2$ from the environment allowing changes in the optical properties of the dielectric layer, thus a shift in the plasmonic resonance peak.

# Chapter 2.

# Literature Review

## 2.1 Classifications of gas sensors

With technology developing more rapidly than ever before, we are on the brink of a technological revolution also known as the Fourth Industrial Revolution. Advances in artificial intelligence (AI), robotics, the Internet of Things (IoT), 3D printing, genetic engineering, quantum computing, and many other technological advancements will soon alter the way we live, work, and relate with one another. Due to these technological developments, gas sensors have been receiving increased attention due to their applications in various intelligent systems. Among other applications, gas sensing technology plays a significant role in areas such as medical[12–14] indoor air quality[15–17] industrial production[18–20] automotive industry[21], and environmental monitoring.[22–24]

However, with the rapid development of technology, there is also a demand for faster, smaller, and more reliable sensors. For this reason, many different studies have been made in developing the most suitable sensor, establishing various branches of gas sensing methods and technologies. Although there are many different classifications of sensors, they can be grouped into two major groups based on their method of detection: [1] methods based on variation in electrical signal with different material and [2] different methods based on other variations. Because most commercial sensors in our society utilizes electrical variant sensors, largely chemoresistive sensors,

most sensor studies are driven towards improving resistive sensors through the use of different materials and other methods including nanostructuring and surface modifications. Hence, sensors based on variation in electrical signal are grouped into one group. On the other hand, the second group consists of every other methods of variations such as optical, calorimetric, and acoustic. Table 2.1 summarizes the classification of different gas sensors based on their method and operating principle.

Recently, among the different classifications of gas sensors, optical sensors, or more specifically sensors that utilize surface plasmon resonance, have received considerable attention. Rapid development of technology provided more precise nanostructure fabrication, which allows control over the surface plasmon resonances, sparking international interest. Localized surface plasmons (LSPs) offer several orders of electric field enhancements that are extremely sensitive to its immediate dielectric surrounding. This makes them attractive for sensing applications as they have the potential for increased sensitivity, fast response times, and lower susceptibility to mechanical failure as they do not require any electrical contact.[25]

**Table 2.1** Classification of gas sensing methods

| Classification | Signal | Advantage | Disadvantage |
|---|---|---|---|
| Resistive | - Change in resistance | - Applicable for wide range of target gases<br>- Short response time<br>- Low cost<br>- Long lifetime | - High power consumption<br>- Sensitive to environment |
| Optical | - Absorbance<br>- Scattering<br>- Fluorescence<br>- Luminescence<br>- Change in refractive index | - High selectivity, sensitivity, and stability<br>- High durability<br>- Short response time | - Difficulty in fabrication<br>- Relatively costly |
| Electrochemical | - Change in current | - High sensitivity<br>- No sensor poisoning<br>- Low power consumption<br>- Good resolution | - Limited temperature range<br>- Short lifetime |
| Gas chromatograph | - Vaporized sample injection into system | - High sensitivity and selectivity<br>- Excellent separation performance | - High cost<br>- Robust and difficult to miniaturize |
| Calorimetric | - Change in temperature due to reaction | - Stable in ambient conditions<br>- Low cost | - Catalyst poisoning<br>- Risk of explosion |
| Acoustic | - Change in velocity of acoustic wave | - Long lifetime<br>- No secondary pollution | - High cost<br>- Difficulty in miniaturization |

## 2.2 Fundamentals of optical gas sensors

### 2.2.1 Types of optical gas sensors

Light-matter interactions can yield a lot of information about any reaction that occurs or the condition of the matter at high speeds. Some of the optical techniques used for measurement include absorbance, luminescence, polarization, interference, time, and wavelength. Optical sensors have attained much attention over the past few decades due to several advantages over commercial sensors such as remote sensing capabilities, no interference from electric or magnetic fields, and wide area of application such as medical diagnostics.[26]

Optical sensors can further be distinguished as extrinsic or intrinsic. The difference between the two depend on the path taken by the radiation. In extrinsic sensors, the radiation is led by the waveguide outside the waveguide and then re-entered into the waveguide to the detector for evaluation. The waveguide simply transports the light to and from the sampling point. On the other hand, in intrinsic sensors, the light never leaves the light guiding structure. The light-guiding structure itself is the sensing element of the sensor.

Optical sensors also have two types of detections that are utilized: direct and indirect (also known as passive or reactive reactions). Like the name implies, for direct detection, the spectroscopic properties of the analyte or the sensing

element are directly observed. Whereas for indirect detection, an additional reagent is used to react with the analyte. Indirect detection often has the opportunity to enhance the selectivity through the use of specific reagents.[26]

Aside from difference in technique, optical sensors can be divided into three categories: [1] modulated parameters, [2] waveguide optics, and [3] analytical detection of the analyte. The two categories of modulated parameters and waveguide optics are defined by transduction principle and determined by the setup of the device, whereas the third depends on the interaction between the analytes and the sensing material. The first two categories can be seen in sensors such as fiber optics and planar waveguide sensors. These types of sensors guide the electromagnetic radiation by internal reflectance. In the third category, sensors such as reflectometric interference spectrography and surface plasmon resonance spectrography are a prime example. In these sensors, the light radiation's interaction with target sample and the analyte are used as a response. The changes in optical properties that occur with the sensor's reaction with the analyte, such as change in thickness and refractive index, are observed as the input. In these sensors, many researcher focus on improving the sensing element material itself more so than the system itself.

### 2.2.2 Plasmonic gas sensor

Plasmonics is a study of light-matter interaction that deal with collective oscillations of conduction electrons excited by electromagnetic radiation. This resonance that occurs on the surface of certain metallic materials is surface plasmon resonance (SPR). As a relatively new and emerging field, plasmonics has enabled a vast array of applications. Used prominently in biological and chemical sensing, plasmonics also have the potential for applications in energy (fuel cells and solar cells)[27,28] data transfer (fiber optics), imaging, and medical diagnosis. As mentioned in Chapter 1, when the material becomes small enough, it creates a localized surface plasmon resonance (LSPR). This aspect of plasmonics will be the basis of this study and the concept behind our plasmonic gas sensors.

Because the full theoretical modeling and explanation of localized surface plasmons is quite long and beyond the scope of this study, just the most important concept on how LSPR is used in sensing and spectroscopic experiments will be discussed. In this study, LSPR scattering is observed to determine sensor response. By observing the shift in LSPR scattering peak wavelength, the sensor's response to target gas could be observed. Our goal is to nanostructure the sensing material in a way that there is enough peak shift to alter the structural color of the sensor itself. The LSPR scattering wavelength maximum, $\lambda_{max}$, is sensitive to the dielectric constant $\varepsilon$ which

is related to the refractive index $n$ by $\varepsilon = n^2$. Therefore, by this relation, any changes in the local environment, which in gas sensor application the adsorption of target gases, should cause a shift in the $\lambda_{max}$. This shift in the LSPR scattering wavelength maximum can be theoretically calculated through the following equation

$$\Delta\lambda_{max} = m\Delta n[1 - \exp\left(-\frac{2d}{l_d}\right)]$$

where $m$ is the bulk refractive index of the nanoparticles, $\Delta n$ is the change in the refractive index due to gas adsorption, $d$ is the analyte absorbate layer thickness, and $l_d$ is the evanescent E-field decay length. This relation is the basis for LSPR wavelength-shift sensing experiments.

## 2.3 Optical Interference

### 2.3.1 Thin film optical interference theory

In an attempt to increase the sensitivity of our sensors, a nanostructure based on thin film optical interference theory was implemented. As mentioned in the Chapter 1, superimposition of two light waves lead to constructive and destructive interferences, which in turn results in interference fringes. When these interference fringes occur on thin structured layers, they can provide vibrant colors called structural colors.[9] In our study, the thickness of $WO_3$ nanorods were varied to form sensors with vibrant colors. Then Au was used as the plasmonic layer due to its strong resonance in the visible light region.[29] When the Au nanoparticle layers are coupled with the constructive fringes, which provides the maximum intensity of superimposed light, the plasmonic effect is greatly enhanced. The interference fringes can be calculated based on the thin-film interference theory below:

$$\frac{m}{2} \times \lambda = 2nd \cos\theta$$

Here the *m* is the interference order with an integer larger than zero, $\lambda$ is the incident wavelength, *n* the refractive index, *d* the film thickness, and $\Theta$ the angle of incident light.

### 2.3.2 Structural colors

By utilizing the thin-film interference theory, the structural colors can be controlled. Although the equation is only viable for thin films, the same theory applies to nanostructures. When the nanostructured sensors based on optical interference are exposed to target gases, the adsorption of these gases should cause a change in the refractive index of the dielectric medium. This, in turn, affects the interference fringe distance. Which enough change, it would cause a displacement large enough that the plasmonic layer is no longer coupled with the constructive fringe. This would result in a drastic change in color.

# Chapter 3.

# Au decorated $WO_3$ thin film on Al mirror layer

## 3.1 Introduction

Within the past decade, environmental issues have become of utmost important throughout the globe. Brought on by the rapid industrialization and population growth, the Earth is suffering from very serious issues of global warming, air and sea pollution, power crisis, and much more. Despite the many efforts in protecting and recovering the environment from pollution, air pollution is still an issue throughout the globe. Nitrogen dioxide ($NO_2$), one of the noxious gases generated from automobiles, factories, and thermal power plants, leads to many environmental problems such as smog and acid rain. Research shows that even at a level of 50 ppb of $NO_2$, long-term exposure is harmful to the heart and the lungs.[30] With the current technological trend towards automated systems and preventative medicine with IoT (Internet of Things) devices, it is important for gas sensors to retain high sensitivity, selectivity and long-term stability with lower power consumption, smaller size, and lower cost for mass production.[31] To realize these evolution, many studies are being made recently in developing sensors utilizing plasmonic resonances.

Tungsten trioxide ($WO_3$) is an n-type semiconductor with a band-gap of 2.6-2.8 eV. $WO_3$ is widely known and studied for its excellent sensitivity and selectivity to a large variety of gas analytes such as $NO_x$ [32,33] $NH_3$,[34] CO,[35] $H_2$,[36,37] and $H_2S$.[38] As a n-type semiconductor, when exposed to

reducing gases its resistance increases whereas oxidizing gases decrease the resistance. For p-type semiconductors, the opposite occurs. A basic summary of the two types of semiconductors is provided in Table 3.1 below.

The response of $WO_3$ is largely dependent on the adsorbed oxygen molecules on its surface. Oxygen on the surface of $WO_3$ is temperature dependent. With increased temperature, the oxygen evolves from $O_2$ to $O_2$- via $O^-$. In another words, all three oxygen species exist on the surface of $WO_3$ and depending on the temperature, one exists more than the other. When the oxygen ion is formed, it forms a barrier to the electron transport. Therefore, when the target gas is introduced to the $WO_3$, the target gas reacts with the oxygen ion. Oxidizing gases causes less electrons leading to stronger barrier, thus the increase in resistance whereas reducing gases decrease the resistance. This is the basic mechanism of $WO_3$, a n-type metal oxide semiconductor.

**Table 3.1** Type of semiconductor and their change in resistance to target gases

| Classification | Oxidizing | Reducing |
|---|---|---|
| n-type | Increase resistance | Decrease resistance |
| p-type | Decrease resistance | Increase resistance |

## 3.2 Sensor fabrication

### 3.2.1 Thin film plasmonic sensor

Aluminum (Al, 500 nm thick) was deposited on Si substrate (1 μm) through the use of thermal evaporator. The substrate was cleaned ultrasonically in acetone, isopropanol, and distilled water followed by drying in nitrogen gas before Al deposition. The $WO_3$ thin film was then deposited on the Al deposited substrate through the electron beam evaporator. The substrate was located 50 cm away from the crucible with a base pressure and deposition rate of and 1.0 Å/s, respectively. The film was then annealed at 300$^{o}$C for 2 h in $N_2$ atmosphere using the tube furnace. Then, 10 nm thick Au film was sequentially deposited at a rate of 0.1 Å/s. The sensor was then annealed at 300$^{o}$C for 10 min through RTA.

## 3.3 Characterization

The morphologies of the Au decorated $WO_3$ thin film on Al mirror layer was characterized by field emission scanning electron microscope (FE-SEM, Zeiss MERLIN Compact) using accelerating voltage of 50 kV. The SEM images of the $WO_3$ thin films are shown in Figure 3.1. The SEM of the thin films show that each film was decorated with extremely small Au nanoparticles on the surface. The nanoparticles seem evenly distributed throughout the film and do not show signs of agglomeration. However, some agglomeration of $WO_3$ can be observed on the film. The cross-sectional images show that the thicknesses are within 3 nm of the intended thickness. The Al layer seems to show different morphology for each sensor. However, it doesn't seem to have much impact on the sensing properties themselves as the Al only plays a part as a mirror layer.

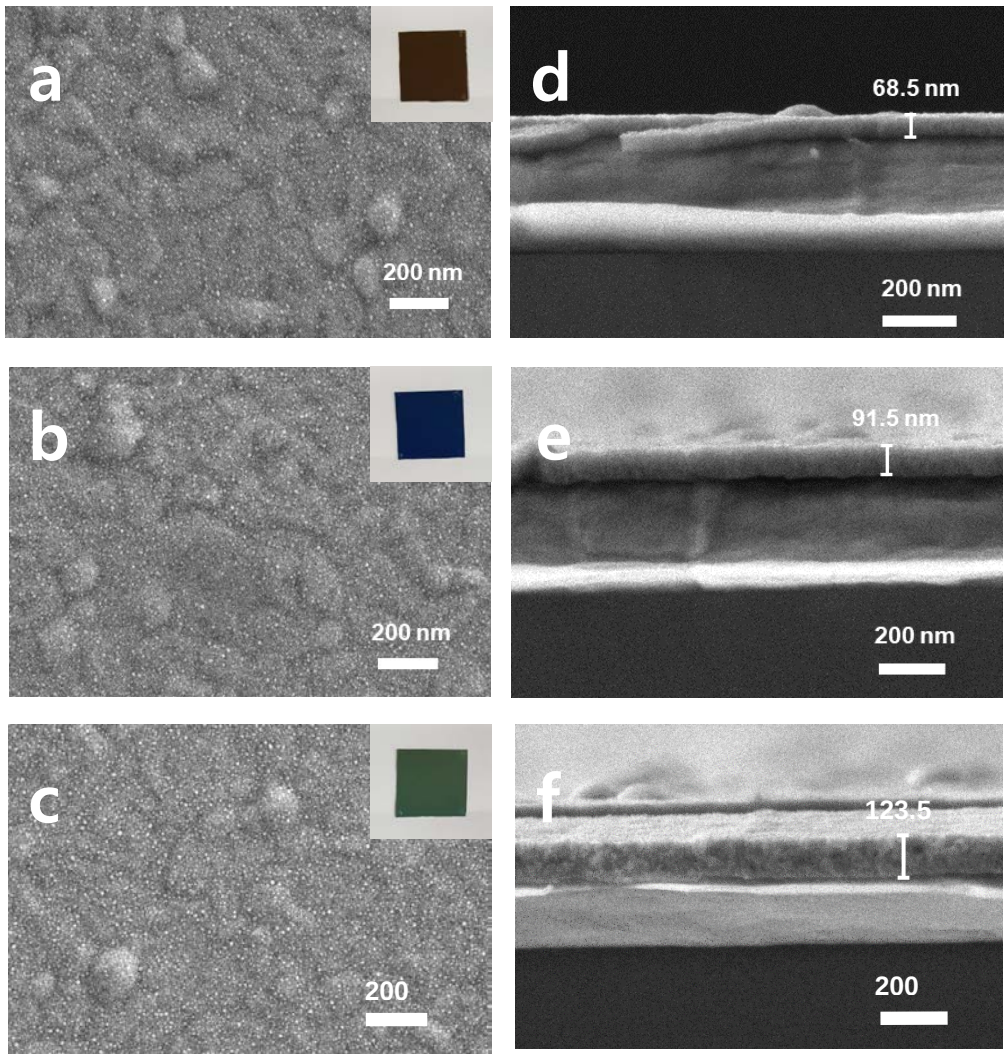


**Figure 3.1** Scanning electron microscopy image of Au decorated $WO_3$ thin film on Al mirror layer. (a-c) Top view of 70 nm, 90 nm, and 130 nm thickness, respectively and the colors of the sensors when observed by the naked eye. (d-f) Cross-sectional view of 70 nm, 90 nm, and 130 nm thickness, respectively.

## 3.4 Finite Difference Time Domain (FDTD) simulation

FDTD simulations were done for $WO_3$ thin film to observe the electromagnetic enhancement and the associated absorbance spectra. With this information, the theoretical structural colors of a certain thickness can be simulated. Figure 3.2 shows the simulation data on Au decorated $WO_3$ thin films and their theoretical structural colors.

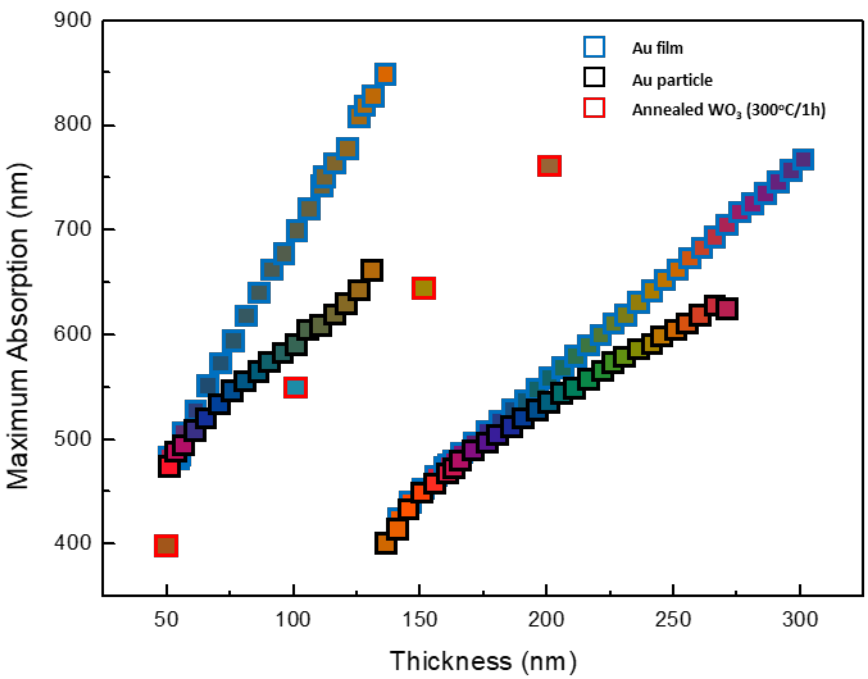


**Figure 3.2** Finite Difference Time Domain simulations of Au decorated $WO_3$ thin film and estimated experimental data for comparison

## 3.5 Gas sensing measurement

### 3.5.1 Optical response

The optical responses of the sensors were measured through the ultraviolet-visible spectrometer (Agilent Cary5000) after being exposed to target gases in a homemade gas flow cell. The cell, equipped for both reflection and transmission measurements, contained a 2 mm thick quartz window on both sides. Stainless steel was used for the body of the cell with two stainless steel gas lines (inlet and outlet) welded into the back side of the cell. A 1 cm spacer was put between the two covers to allow enough space for the sensors to be put in, but not too much to minimize the distance of the sample from the spectrometer measurement window. Figure 3.2 illustrates the flow cell used in this experiment and Figure 3.3 shows the schematic of the experimental setup.

The scattering spectra of the sensor before and after target gas exposure were taken from 300 nm to 800 nm. The gas flow was controlled by mass flow controllers with a continuous flow of 1000 sccm. $NO_2$ concentration of 10 ppm was injected into the flow cell for a period of 500 s. Afterward, inlet and outlet lines were close to create a closed system for the sensor before the optical measurements were taken. The normalized reflectance spectra are shown in Figure 3.4.

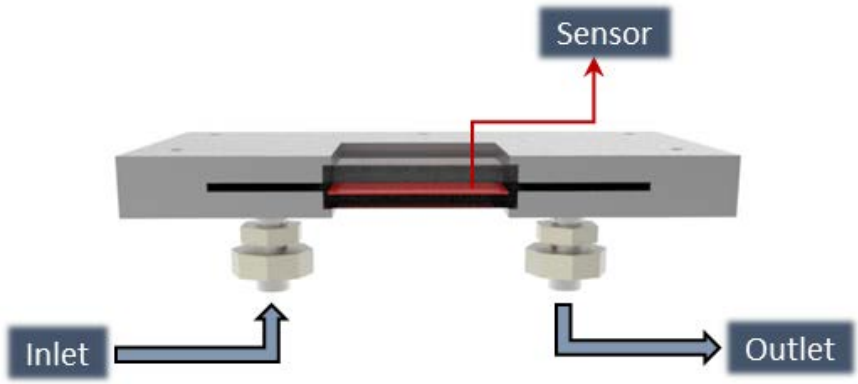


**Figure 3.3** Flow cell for optical response measurement

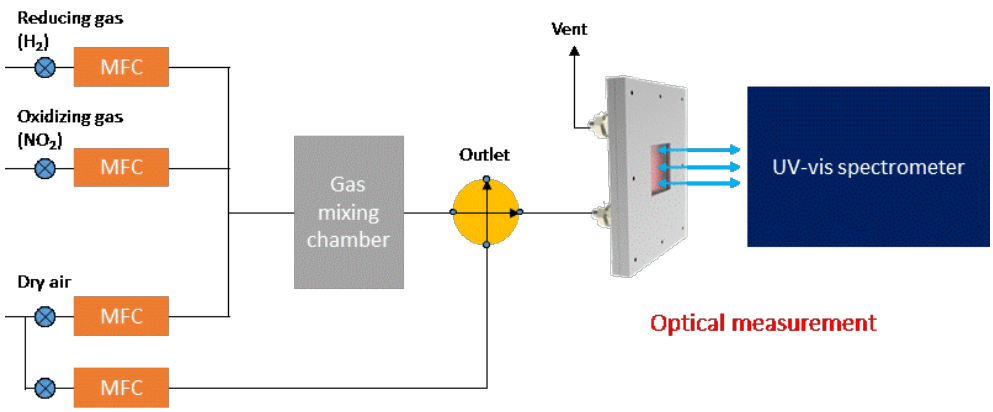


**Figure 3.4** Gas sensing setup for optical response measurement

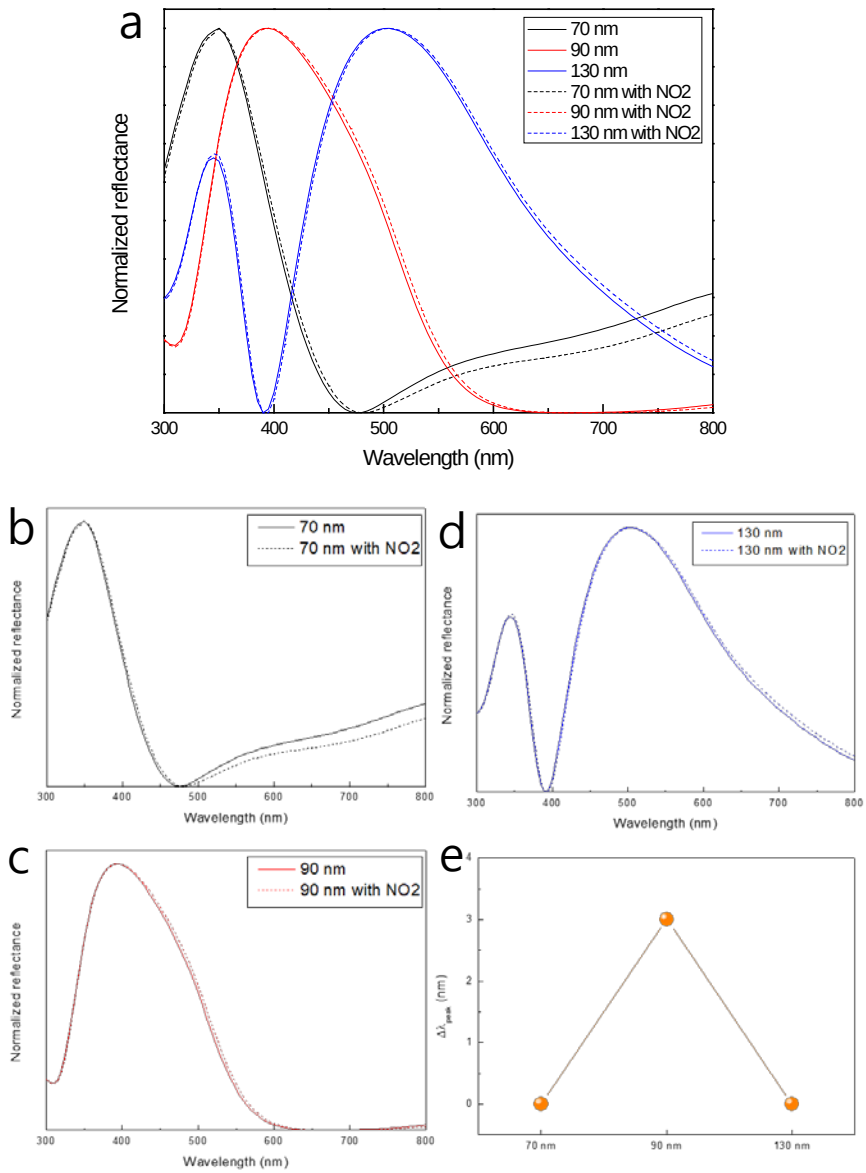


**Figure 3.5** (a) Normalized reflectance measurement of $NO_2$ exposed 70 nm, 90 nm, and 130 nm Au decorated $WO_3$ thin film on Al mirror layer. (b-c) Normalized reflectance spectra separately. (e) Peak shift of the three films.

## 3.6 Conclusion

The Au decorated $WO_3$ thin film sensor was fabricated through electron beam evaporation on Al deposited Si substrate. The variation in $WO_3$ film thickness allowed the fabrication of sensors close to red, blue, and green in color. With more deposition and optimization, fabrication of sensors of any color in the visible spectrum is a possibility.

The optical measurements of the $WO_3$ thin films show very slight shift in the peak wavelength. As shown in Figure 3.5(e), the 90 nm thick $WO_3$ thin film showed the highest peak shift of approximately 3 nm out of the three thicknesses. The lack of peak shift may be due to the operating temperature of the sensing material. $WO_3$ is known to have the most optimal operating temperature of around 200$^{o}$C.[39] Therefore, sufficient adsorption of gas analytes at room temperature may be difficult. Also, even if the target gas successfully adsorbed onto the sensing material, the recovery of the sensor might be difficult.

# Chapter 4.

# Au/Pd decorated $WO_3$ Nanorods on Al mirror layer

## 4.1 Introduction

Excessive use of fossil fuels in our current global society has accelerated global warming due to accumulation of greenhouse gases. Oil, coal, and natural gas are massively utilized for automobiles, factories, and power plants accelerating the issue more. However, unlike fossil fuels, hydrogen does not generate carbon dioxide when combusted. It is a clean and sustainable energy carrier. Therefore, there are many efforts in developing a hydrogen-based economy, creating a cleaner environment by reducing carbon emissions. The ultimate goal of hydrogen economy is the production of hydrogen while generating minimal greenhouse gases, developing infrastructure for hydrogen storage and transport, and the use of fuel cells to harness its energy.

However, one issue that may arise from such economy is that at a certain concentration range of hydrogen, it is highly flammable. Therefore, with the advancement of hydrogen energy, hydrogen sensors will play a critical role. Due to the highly flammable nature of hydrogen, leaks in the storage systems, vehicles and appliances need to be detected immediately. Therefore, hydrogen sensor performance targets specify a response time of 1 s at room temperature for concentrations of 0.1% to 10%.[40] This makes plasmonic sensors highly attractive for such application as optical signals do not generate spark. Like many other hydrogen sensor platforms, Pd will be utilized as the functioning material. Pd is widely used due to its ability to

dissociate hydrogen gas efficiently at ambient conditions and its reversible phase transformation from metal to metal hydride at room temperature. Therefore, Pd decoration on $WO_3$ nanorods, another material capable of hydrogen sensing, will be used for plasmonic gas sensing of hydrogen.

In Table 4.1, a review of current studies on hydrogen sensors are summarized and compared to this study. Although this is based on the resistive response of the sensors, we believe that the nanostructure for plasmonic optical interference has potential to become a highly sensitive hydrogen sensor

**Table 4.1** $H_2$ detection using various types of gas sensors based on $WO_3$

| | Sensing materials | $H_2$ concentration | S (Rgas/Rair or Rair/Rgas) | Working temperature | Fabrication method | Reference |
|---|---|---|---|---|---|---|
| 1 | Pd/$WO_3$ nanowires | 0.1% | 3.1 | 300 | Drop-casting of Pd-functionalized $WO_3$ nanowires | 41 |
| 2 | 10% mol Pd/$WO_3$ | 500 ppm | 30 | 300 | Electro-spinning | 42 |
| 3 | Pd/$WO_3$ films | 1300 ppm | 100 | 200 | Sol-gel process | 43 |
| 4 | Pd doped $WO_3$ nanowires | 200 ppm | 69 | 180 | Hydrothermal (nanowires), Precipitation ($WO_3$ nanospheres), Flow through protonated ion exchange in acidic solution ($WO_3$ nanolamelle) Screen printing (sensors) | 44 |
| 5 | Unloaded $WO_3$ | 1000 ppm | 13.6 | 300 | Reactive magnetron sputtering (sensors) | 45 |
| 6 | $WO_3$ nanodots | 1000 ppm | 79 | 200 | Electrochemical anodizing | 46 |
| 7 | MWCNT-doped $WO_3$ | 1000 | 3 | 350 | Electron beam evaporation | 19 |
| 8 | Pt-doped | 200 ppm | 9.5 | 200 | RF magnetron | 19 |

| | | | | | | |
|---|---|---|---|---|---|---|
| | $WO_3$ | | | | sputtering | |
| 9 | Pt-loaded $WO_3$ | 1 vol% | 200 | 150 | RF magnetron sputtering | 36 |
| 10 | 1.0 wt% Pd-loaded $WO_3$ | 200 ppm | 16219.8 | 200 | Screen printing | 47 |
| 11 | Pd/$WO_3$ nanoparticles | 500 ppm | 78 | 100 | Hydrothermal | 48 |
| 12 | Pt-loaded $WO_3$ | 500 ppm | 0.02 | 150 | Reactive rf sputtering | 48 |
| 13 | Unloaded $WO_3$ | 1000 ppm | 13.6 | 300 | Reacitve magnetron sputtering | 45 |
| 14 | **Pd decorated $WO_3$ nanorods** | **50 ppm** | **260000** | **150** | **GlAD ($WO_3$ nanorods), solution process (Pd nanoparticle)** | **This Work** |

## 4.2 Sensor fabrication

### 4.2.1 Resistive sensor with nanorods

Interdigitated electrodes (IDEs) of platinum (Pt, 150 nm thick) and titanium (Ti, 30 nm thick) were patterned with spacing of 4 µm on $SiO_2$/Si substrate (1 µm/550 µm thick) using photolithography. Before deposition of the sensing material, the IDE patterned substrate was cleaned ultrasonically in acetone, isopropanol, and distilled water followed by drying in nitrogen gas. A mask was attached to the substrate for the deposition of the $WO_3$ nanorod in just the sensing area. The evaporation of $WO_3$ was carried out at a glancing angle of $80^o$ with a rotation speed of 80 rpm. The base pressure and growth rate were $3x10^{-6}$ and 1.0 Å/s, respectively. A $WO_3$ seed layer of 20 nm was deposited at $0^o$ at a rate of 1.0 Å/s for a uniform growth of the nanorods. The seed layer also assisted in the passivation of the Al layer from further oxidation and corrosion. The substrate was then annealed at $300^oC$ for 2 h in $N_2$ atmosphere using the tube furnace. The annealed substrate was then decorated with Pd nanoparticles through wet chemistry. A water bath of $70^oC$ was prepared for the synthesis. Pd salt solution of 5 mg potassium tetrachloropalladate(II) was dissolved in 50 mg of distilled water. The substrate was dipped in the Pd salt solution, which was kept stirring at the water bath temperature. The substrate was kept in the solution for 1 min which was rinsed with DI water and dried with $N_2$ gas once taken out. The Pd

decorated substrate was then annealed in 300$^{o}$C for 10 min through the rapid thermal annealing (RTA) system, functionalizing the Pd NPs. Then, 10 nm thick Au film was sequentially deposited at a rate of 0.1 Å/s. The sensor was then annealed at 300$^{o}$C for 10 min through RTA

### 4.2.2 Plasmonic sensor with nanorods

Aluminum (Al, 500 nm thick) was deposited on Si substrate (1 μm) through the use of thermal evaporator. The substrate was cleaned ultrasonically in acetone, isopropanol, and distilled water followed by drying in nitrogen gas before Al deposition. Then, the $WO_3$ nanorods were deposited through the GLAD system based on an electron beam evaporator. To fabricate the $WO_3$ nanorods, the evaporation of $WO_3$ was carried out at a glancing angle of 80$^{o}$ with a rotation speed of 80 rpm. The base pressure and growth rate were $3x10^{-6}$ and 1.0 Å/s, respectively. A $WO_3$ seed layer of 20 nm was deposited at 0$^{o}$ at a rate of 1.0 Å/s for a uniform growth of the nanorods. The seed layer also assisted in the passivation of the Al layer from further oxidation and corrosion. The substrate was then annealed at 300$^{o}$C for 2 h in $N_2$ atmosphere using the tube furnace. The annealed substrate was then decorated with Pd nanoparticles through wet chemistry. A water bath of 70$^{o}$C was prepared for the synthesis. Pd salt solution of 5 mg potassium tetrachloropalladate(II) ($K_2PdCl_4$) was dissolved in 50 mg of distilled water. The substrate was dipped in the Pd salt solution, which was kept stirring at the water bath temperature.

The substrate was kept in the solution for 1 min which was rinsed with DI water and dried with $N_2$ gas once taken out. The Pd decorated substrate was then annealed in 300$^oC$ for 10 min through the rapid thermal annealing (RTA) system. Then, 10 nm thick Au film was sequentially deposited at a rate of 0.1 Å/s. The sensor was then annealed at 300$^oC$ for 10 min through RTA.

## 4.3 Characterization

The morphologies of the Au/Pd decorated $WO_3$ nanorods were characterized by field emission scanning electron microscope (FE-SEM, Zeiss MERLIN Compact) using accelerating voltage of 50 kV. The SEM images of the Au/Pd decorated $WO_3$ nanorods are shown in Figure 4.1. The images show that entire surface of the nanorods are decorated with small Pd nanoparticles, less than 30 nm in size. Au can be seen agglomerated on top of the nanorods in the top view images. The cross-sectional images show that the thicknesses of the nanorods were slightly varied. Some optimization is needed for better control of the deposition.

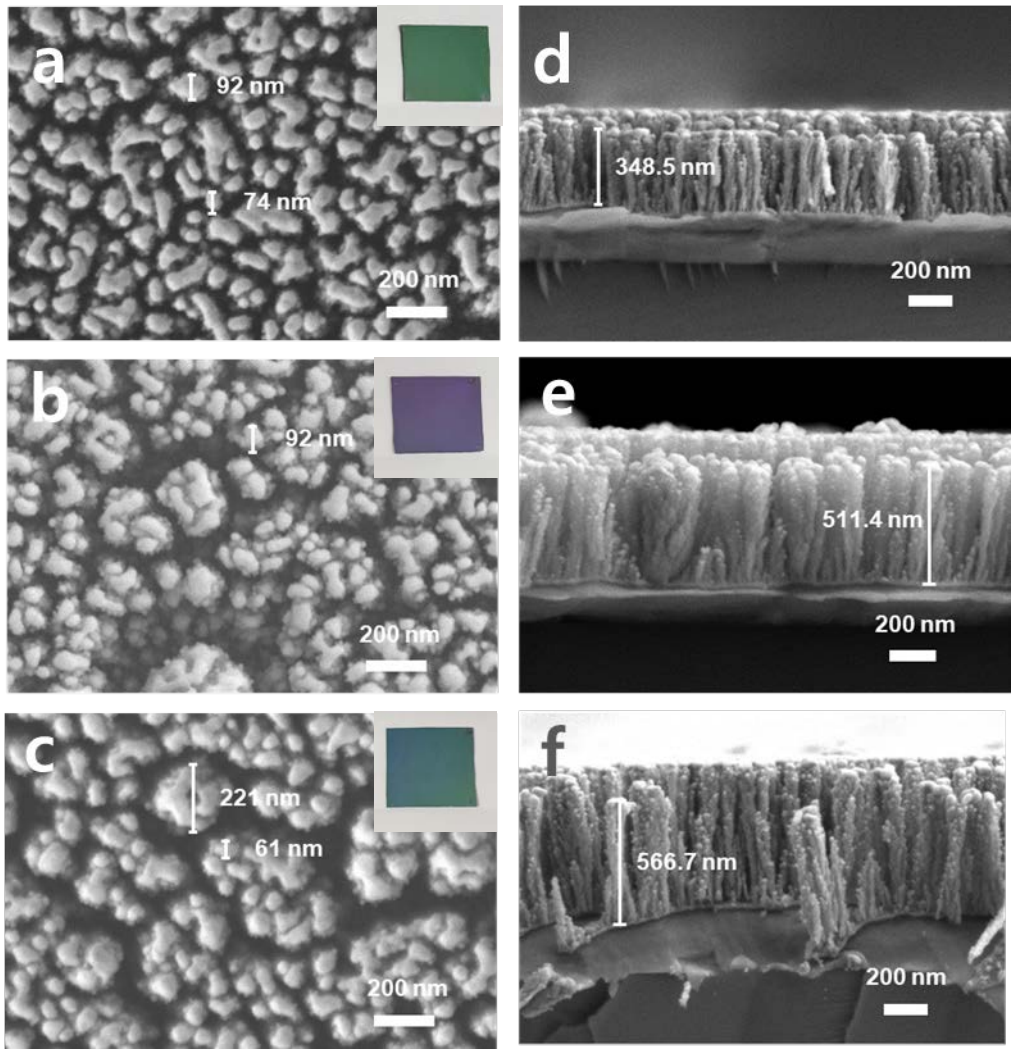


**Figure 4.1** Scanning electron microscopy image of Au/Pd decorated $WO_3$ nanorods on Al mirror layer. (a-c) Top view of 300 nm, 400 nm, and 500 nm thickness, respectively and the colors of the sensors when observed by the naked eye. (d-f) Cross-sectional view of 300 nm, 400 nm, and 500 nm thickness, respectively.

## 4.4 Gas sensing measurement

### 4.4.1 Resistive response

The gas sensing properties of the Au/Pd decorated $WO_3$ nanorods were measured in a box furnace at room temperature, 100°C, 150°C, 200°C, and 250°C. The resistance changes were measured by changing the flow of gas from dry air to target gas (dry air balance, Sinjin Gases) under a DC bias volage of 1V using a source measurement unit (Keithley236). Mass flow controllers were used to control the amount of dry air and target gas in a continuous flow of 1000 sccm. The response was calculated after the sensor was fully saturated and stabilized.

The response of the resistive sensor is defined as the ratio of the resistance before and after gas exposure as shown in the following equations.

$$Response = \frac{R_g}{R_a} \; or \; Response = \frac{R_a}{R_g}$$

$$Response\ (\%) = \frac{\Delta R}{R_g} \times 100\ (\%)$$

Where Ra is the resistance of the sensor in ambient conditions and Rg is the resistance in target gas, and $\Delta R = |R_a - R_g|$. Sensitivity of the sensor is defined as the change in measured signal per analyte concentration.

The response time is the time it takes the sensor to go from 10% to 90% of

the equilibrium value upon exposure to target gas. Recovery is the time it takes for the sensor to return to the 90% of its initial value when target gas is removed.

The chemoresistive response was first performed to check the activity of Pd in various temperature levels. Like predicted, the sensor showed very little response to target gas at room temperature. However, when checked under higher temperatures, the sensor showed remarkable response. The sensor response at room temperature and at 150$^{o}$C is shown in Figure 4.2

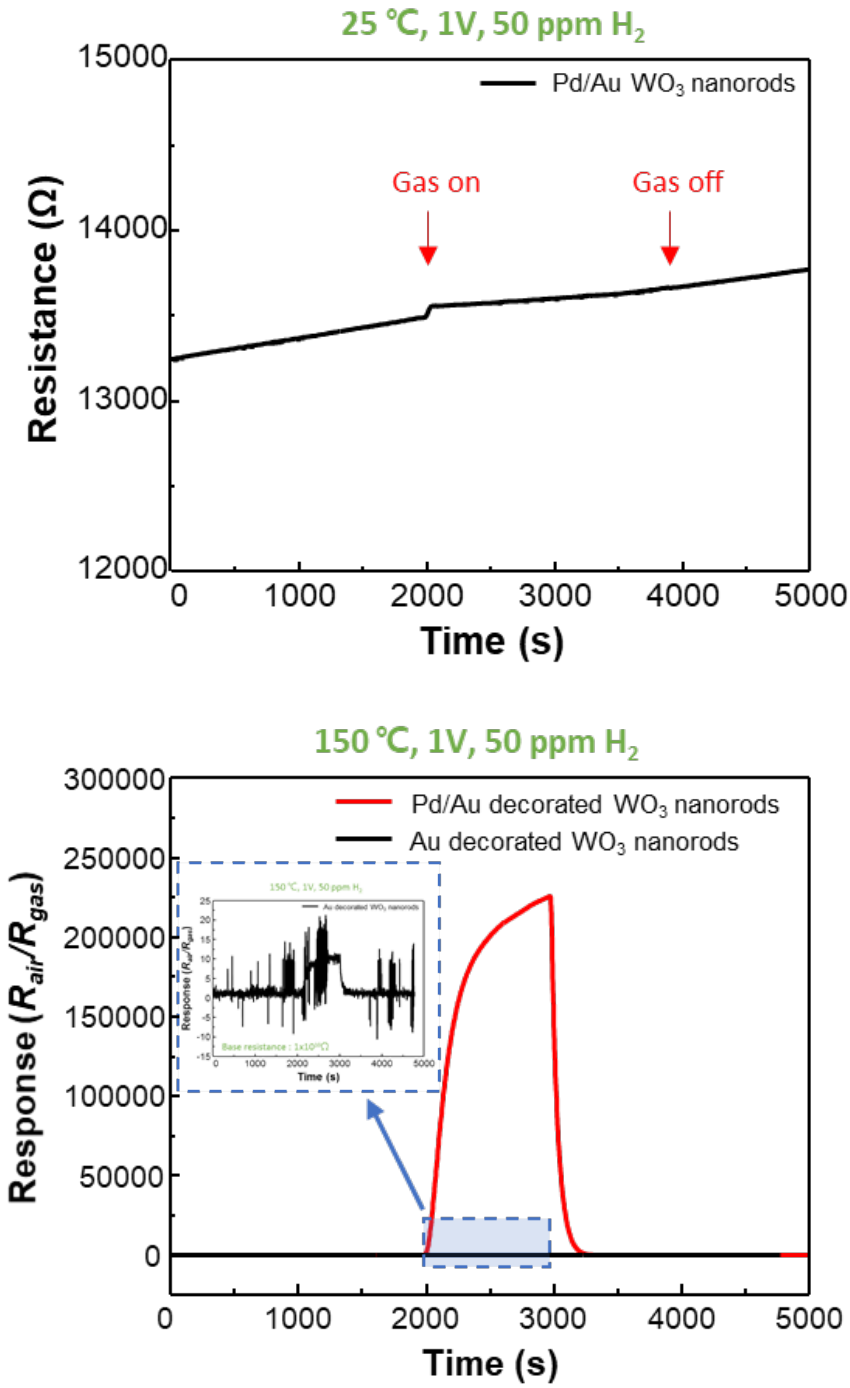


**Figure 4.2** Resistive gas sensing at room temperature and 150°C

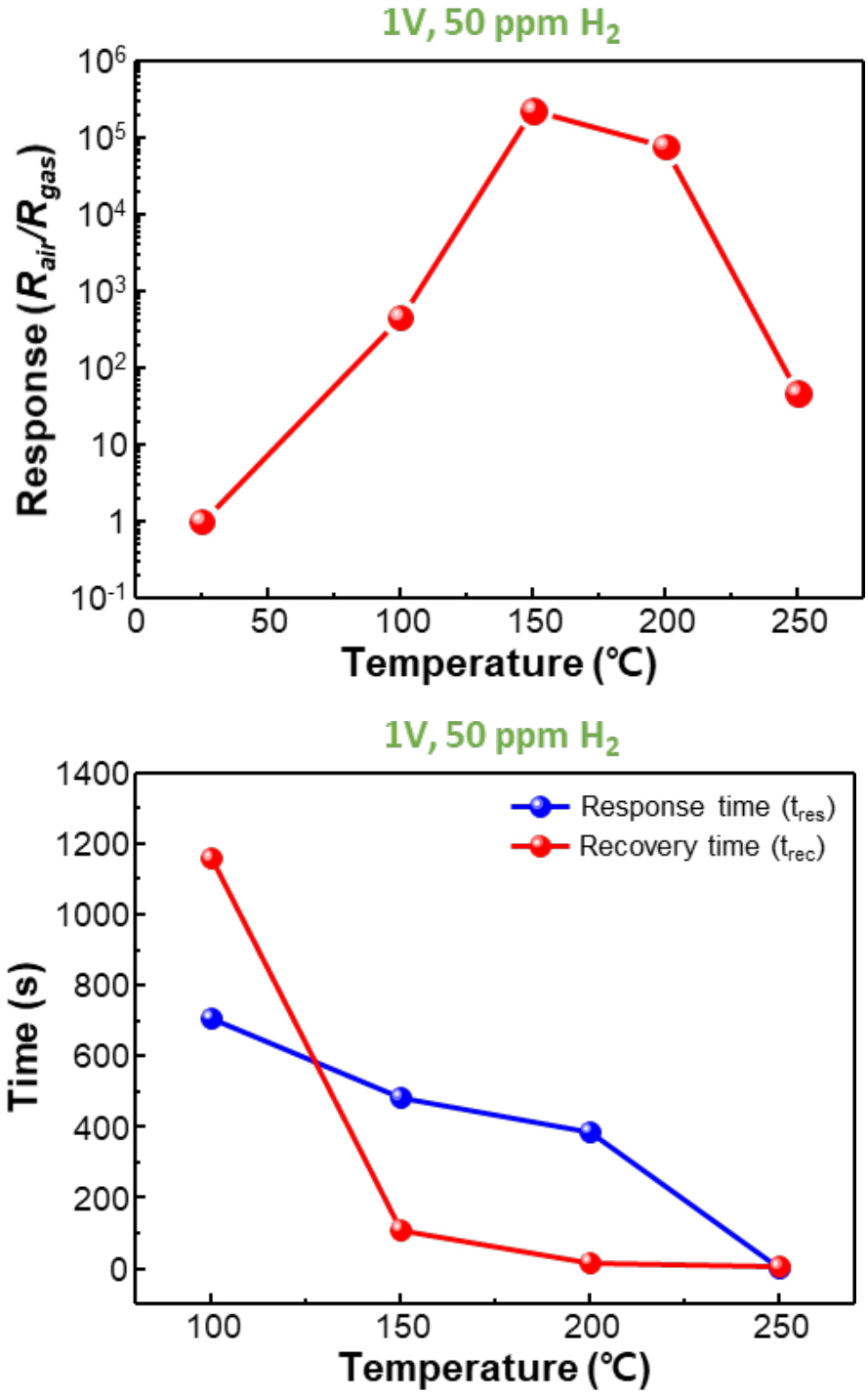


**Figure 4.3** (a) Gas sensing response at 25°C, 100°C, 150°C, 200°C, and 250°C.

(b) Response time and recovery time at 100°C, 150°C, 200°C, and 250°C.

### 4.4.2 Optical response

The optical responses of the sensors were measured through the ultraviolet-visible spectrometer (Agilent Cary5000) after being exposed to target gases in a homemade gas flow cell. The cell, equipped for both reflection and transmission measurements, contained a 2 mm thick quartz window on both sides. Stainless steel was used for the body of the cell with two stainless steel gas lines (inlet and outlet) welded into the back side of the cell. A 1 cm spacer was put between the two covers to allow enough space for the sensors to be put in, but not too much to minimize the distance of the sample from the spectrometer measurement window.

The scattering spectra of the sensor before and after target gas exposure were taken from 300 nm to 800 nm. $H_2$ concentration of 50 ppm and $NO_2$ concentrations of 10 ppm were injected into the flow cell for 500 s before the lines were closed to create a close system in the flow cell for two separate optical measurements. The gas flow was controlled by mass flow controllers with a continuous flow of 1000 sccm. The normalized reflectance spectra based on $H_2$ exposure are shown in Figure 4.2 and the normalized reflectance spectra based on $NO_2$ exposure are shown in Figure 4.3

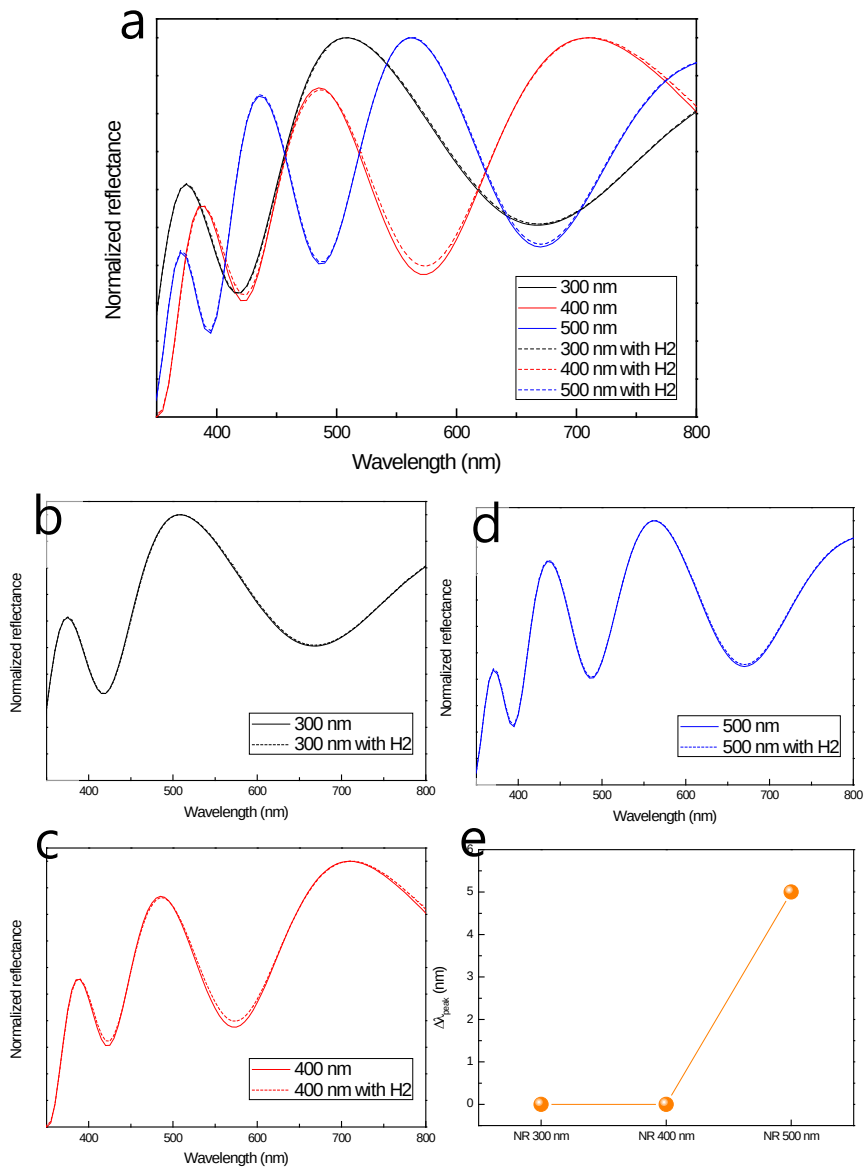


**Figure 4.4** (a) Normalized reflectance measurement of $H_2$ exposed 300 nm, 400 nm, and 500 nm Au/Pd decorated $WO_3$ thin film on Al mirror layer. (b-c) Normalized reflectance spectra separately. (e) Peak shift of the three films.

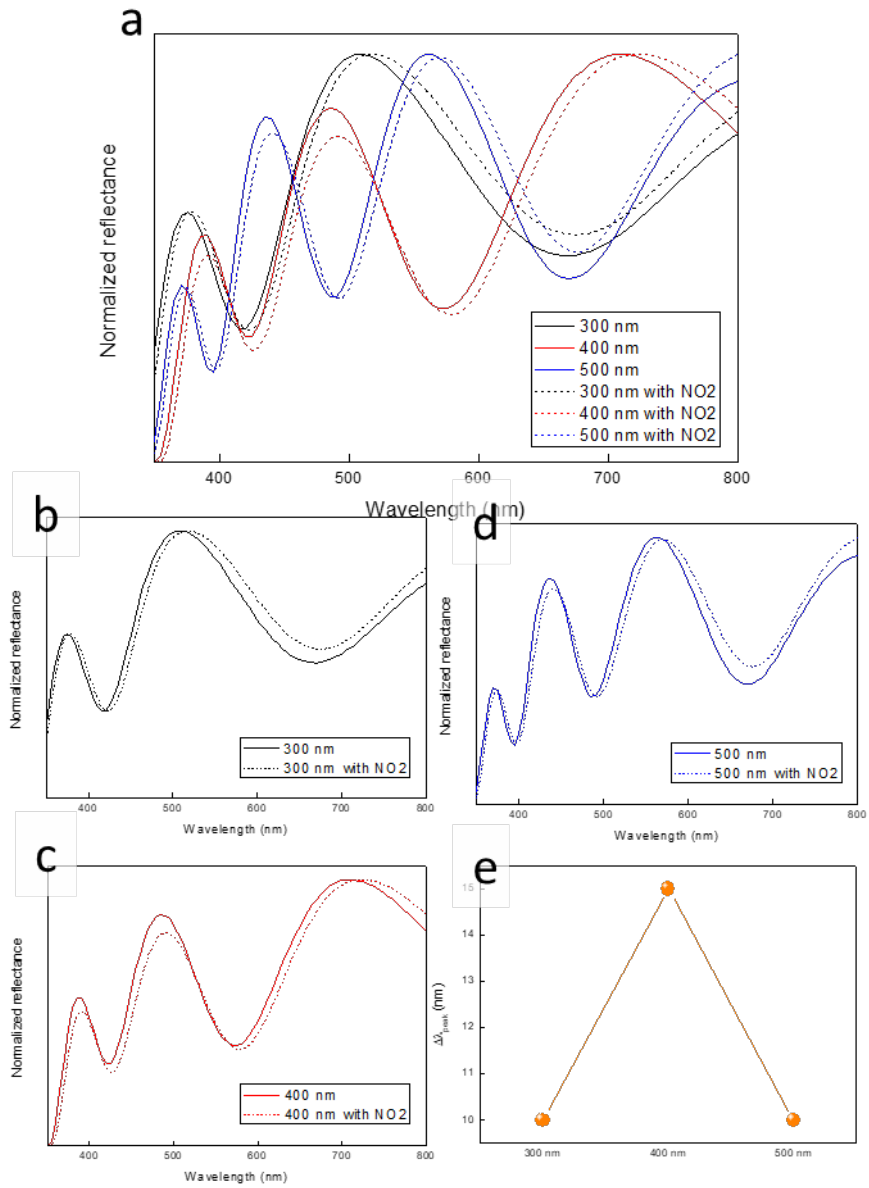


**Figure 4.5** (a) Normalized reflectance measurement of $NO_2$ exposed 300 nm, 400 nm, and 500 nm Au/Pd decorated $WO_3$ thin film on Al mirror layer. (b-c) Normalized reflectance spectra separately. (e) Peak shift of the three films.

## 4.5 Conclusion

The Au/Pd decorated $WO_3$ nanorods sensor was fabricated through the glancing angle deposition (GLAD) method using the electron beam evaporator. The $WO_3$ was deposited onto an Al deposited Si substrate which was subsequently decorated with Pd through wet chemistry synthesis method after annealing. After the Pd NPs were functionalized through annealing, Au was deposited and once again annealed to agglomerate the Au NPs on the surface of the $WO_3$ nanorods. Like the thin films, the variation in the thickness of the nanorods allowed fabrication of various structural colors. The nanostructure was also deposited onto IDE for resistive gas sensing measurement

# Chapter 5.

# Summary

## 5.1 Summary

In this study, plasmonic gas sensor was fabricated utilizing the concept of optical interference coupled with the electromagnetic enhancement of plasmon resonances. The localized surface plasmon resonance (LSPR) and surface plasmon polariton (SPP) caused by the interaction of light with the plasmonic layer of the sensor is utilized in fabricating sensors of various structural colors. The resonances that occur at the plasmonic layers of the sensors are extremely sensitive to changes in its environment. Therefore, tungsten dioxide ($WO_3$) nanorods were decorated with Pd nanoparticles for $NO_2$ and $H_2$ detection. The adsorption of the target gases caused a slight shift in the peak wavelength of the sensors. The resistive gas sensing showed that the nanostructured material itself is highly responsive to hydrogen on a competitive level with current sensors. Therefore, the sensors in this study shows promise as a potential hydrogen and $NO_2$ sensor.

# References


(1) Seiyama, T.; Kagawa, S. Study on a Detector for Gaseous Components Using Semiconductive Thin Films. *Anal. Chem.* **1966**, *38* (8), 1069–1073. https://doi.org/10.1021/ac60240a031.

(2) Burgués, J.; Marco, S. Low Power Operation of Temperature-Modulated Metal Oxide Semiconductor Gas Sensors. *Sensors (Switzerland)* **2018**, *18* (2). https://doi.org/10.3390/s18020339.

(3) Prades, J. D.; Jimenez-Diaz, R.; Hernandez-Ramirez, F.; Barth, S.; Cirera, A.; Romano-Rodriguez, A.; Mathur, S.; Morante, J. R. Ultralow Power Consumption Gas Sensors Based on Self-Heated Individual Nanowires. *Appl. Phys. Lett.* **2008**, *93* (12). https://doi.org/10.1063/1.2988265.

(4) Comini, E.; Faglia, G.; Sberveglieri, G.; Pan, Z.; Wang, Z. L. Stable and Highly Sensitive Gas Sensors Based on Semiconducting Oxide Nanobelts. *Appl. Phys. Lett.* **2002**, *81* (10), 1869–1871. https://doi.org/10.1063/1.1504867.

(5) Guidi, V.; Cardinali, G. C.; Dori, L.; Faglia, G.; Ferroni, M.; Martinelli, G.; Nelli, P.; Sberveglieri, G. Thin-Film Gas Sensor Implemented on a Low-Power-Consumption Micromachined Silicon

Structure. *Sensors Actuators, B Chem.* **1998**, *49* (1–2), 88–92. https://doi.org/10.1016/S0925-4005(98)00039-2.

(6) Zhan, Z.; Jiang, D.; Xu, J. Investigation of a New In2O3-Based Selective H 2 Gas Sensor with Low Power Consumption. *Mater. Chem. Phys.* **2005**, *90* (2–3), 250–254. https://doi.org/10.1016/j.matchemphys.2004.01.043.

(7) Xu, X.; Fan, H.; Liu, Y.; Wang, L.; Zhang, T. Au-Loaded In2O3 Nanofibers-Based Ethanol Micro Gas Sensor with Low Power Consumption. *Sensors Actuators, B Chem.* **2011**, *160* (1), 713–719. https://doi.org/10.1016/j.snb.2011.08.053.

(8) Sur, U. K. Surface-Enhanced Raman Spectroscopy. *Resonance* **2010**, *15* (2), 154–164. https://doi.org/10.1007/s12045-010-0016-6.

(9) Choi, D.; Shin, C. K.; Yoon, D.; Chung, D. S.; Jin, Y. W.; Lee, L. P. Plasmonic Optical Interference. *Nano Lett.* **2014**, *14* (6), 3374–3381. https://doi.org/10.1021/nl5008823.

(10) Adams, B. D.; Chen, A. The Role of Palladium in a Hydrogen Economy. *Mater. Today* **2011**, *14* (6), 282–289. https://doi.org/10.1016/S1369-7021(11)70143-2.

(11) Favier, F.; Walter, E. C.; Zach, M. P.; Benter, T.; Penner, R. M. Hydrogen Sensors and Switches from Electrodeposited Palladium

Mesowire Arrays. *Science (80-. ).* **2001**, *293* (5538), 2227–2231. https://doi.org/10.1126/science.1063189.

(12) McKinley, B. A.; Lee Parmley, C. Preliminary Clinical Trial of an Ex Vivo Arterial Blood Gas Monitor. *J. Crit. Care* **2004**, *12* (4), 214–220. https://doi.org/10.1016/s0883-9441(97)90035-6.

(13) Song, K.; Wang, Q.; Liu, Q.; Zhang, H.; Cheng, Y. A Wireless Electronic Nose System Using a Fe2O3 Gas Sensing Array and Least Squares Support Vector Regression. *Sensors* **2011**, *11* (1), 485–505. https://doi.org/10.3390/s110100485.

(14) Lilienthal, A. J.; Loutfi, A.; Duckett, T. Airborne Chemical Sensing with Mobile Robots. *Sensors* **2006**, *6* (11), 1616–1678. https://doi.org/10.3390/s6111616.

(15) Ke, M.-T.; Lee, M.-T.; Lee, C.-Y.; Fu, L.-M. A MEMS-Based Benzene Gas Sensor with a Self-Heating WO3 Sensing Layer. *Sensors* **2009**, *9* (4), 2895–2906. https://doi.org/10.3390/s90402895.

(16) Kim, K. S.; Baek, W. H.; Kim, J. M.; Yoon, T. S.; Lee, H. H.; Kang, C. J.; Kim, Y. S. A Nanopore Structured High Performance Toluene Gas Sensor Made by Nanoimprinting Method. *Sensors* **2010**, *10* (1), 765–774. https://doi.org/10.3390/s100100765.

(17) Bakrania, S. D.; Wooldridge, M. S. The Effects of the Location of Au

Additives on Combustion-Generated SnO2 Nanopowders for Co Gas Sensing. *Sensors* **2010**, *10* (7), 7002–7017. https://doi.org/10.3390/s100707002.

(18) Anderson, T.; Ren, F.; Pearton, S.; Kang, B. S.; Wang, H. T.; Chang, C. Y.; Lin, J. Advances in Hydrogen, Carbon Dioxide, and Hydrocarbon Gas Sensor Technology Using GaN and ZnO-Based Devices. *Sensors (Switzerland)* **2009**, *9* (6), 4669–4694. https://doi.org/10.3390/s90604669.

(19) Wongchoosuk, C.; Wisitsoraat, A.; Phokharatkul, D.; Tuantranont, A.; Kerdcharoen, T. Multi-Walled Carbon Nanotube-Doped Tungsten Oxide Thin Films for Hydrogen Gas Sensing. *Sensors* **2010**, *10* (8), 7705–7715. https://doi.org/10.3390/s100807705.

(20) Alfeeli, B.; Pickrell, G.; Wang, A. Sub-Nanoliter Spectroscopic Gas Sensor. *Sensors* **2006**, *6* (10), 1308–1320. https://doi.org/10.3390/s6101308.

(21) Endres, H. E.; Hartinger, R.; Drost, S.; Hellmich, W.; Müller, G.; Bosch-v. Braunmühl, C.; Krenkow, A.; Perego, C.; Sberveglieri, G.; Göttler, W. A Thin-Film SnO2 Sensorsystem for Simultaneous Detection of CO and NO2 with Neural Signal Evaluation. *VDI Berichte* **1996**, *36* (1255), 149–154.

(22) Papadopoulos, C. A.; Avaritsiotis, J. N. A Model for the Gas Sensing Properties of Tin Oxide Thin Films with Surface Catalysts. *Sensors Actuators B. Chem.* **1995**, *28* (3), 201–210. https://doi.org/10.1016/0925-4005(95)01728-3.

(23) Binions, R.; Naik, A. J. T. Metal Oxide Semiconductor Gas Sensors in Environmental Monitoring. *Semicond. Gas Sensors* **2013**, No. x, 433–466. https://doi.org/10.1533/9780857098665.4.433.

(24) Chen, I. C.; Lin, S. S.; Lin, T. J.; Hsu, C. L.; Hsueh, T. J.; Shieh, T. Y. The Assessment for Sensitivity of a NO2 Gas Sensor with ZnGa2O4/ZnO Core-Shell Nanowires-a Novel Approach. *Sensors* **2010**, *10* (4), 3057–3072. https://doi.org/10.3390/s100403057.

(25) Powell, A. W.; Coles, D. M.; Taylor, R. A.; Watt, A. A. R.; Assender, H. E.; Smith, J. M. Plasmonic Gas Sensing Using Nanocube Patch Antennas. *Adv. Opt. Mater.* **2016**, *4* (4), 634–642. https://doi.org/10.1002/adom.201500602.

(26) Rathgeb, F.; Gauglitz, G. Optical Gas Sensors in Analytical Chemistry: Applications, Trends and General Comments. *Encycl. Anal. Chem.* **2006**, 1–15. https://doi.org/10.1002/9780470027318.a0709.

(27) Kim, S.; Yu, Y.; Jeong, S. Y.; Lee, M. G.; Jeong, H. W.; Kwon, Y.

M.; Baik, J. M.; Park, H.; Jang, H. W.; Lee, S. Plasmonic Gold Nanoparticle-Decorated BiVO 4 /ZnO Nanowire Heterostructure Photoanodes for Efficient Water Oxidation. *Catal. Sci. Technol.* **2018**, *8* (15), 3759–3766. https://doi.org/10.1039/c8cy00685g.

(28) Lee, M. G.; Moon, C. W.; Park, H.; Sohn, W.; Kang, S. B.; Lee, S.; Choi, K. J.; Jang, H. W. Dominance of Plasmonic Resonant Energy Transfer over Direct Electron Transfer in Substantially Enhanced Water Oxidation Activity of BiVO4 by Shape-Controlled Au Nanoparticles. *Small* **2017**, *13* (37), 1–11. https://doi.org/10.1002/smll.201701644.

(29) Yamada, K.; Miyajima, K.; Mafuné, F. Thermionic Emission of Electrons from Gold Nanoparticles by Nanosecond Pulse-Laser Excitation of Interband. *J. Phys. Chem. C* **2007**, *111* (30), 11246–11251. https://doi.org/10.1021/jp0730747.

(30) Kim, T. H.; Hasani, A.; Quyet, L. Van; Kim, Y.; Park, S. Y.; Lee, M. G.; Sohn, W.; Nguyen, T. P.; Choi, K. S.; Kim, S. Y.; et al. NO 2 Sensing Properties of Porous Au-Incorporated Tungsten Oxide Thin Films Prepared by Solution Process. *Sensors Actuators, B Chem.* **2019**, *286* (2), 512–520. https://doi.org/10.1016/j.snb.2019.02.009.

(31) Joy, N. A.; Nandasiri, M. I.; Rogers, P. H.; Jiang, W.; Varga, T.; Kuchibhatla, S. V. N. T.; Thevuthasan, S.; Carpenter, M. A. Selective

Plasmonic Gas Sensing: H 2 , NO 2 , and CO Spectral Discrimination by a Single Au-CeO 2 Nanocomposite Film. *Anal. Chem.* **2012**, *84* (11), 5025–5034. https://doi.org/10.1021/ac3006846.

(32) Khatko, V.; Vallejos, S.; Calderer, J.; Gracia, I.; Cané, C.; Llobet, E.; Correig, X. Micro-Machined WO3-Based Sensors with Improved Characteristics. *Sensors Actuators, B Chem.* **2009**, *140* (2), 356–362. https://doi.org/10.1016/j.snb.2009.05.020.

(33) Liu, Z.; Yamazaki, T.; Shen, Y.; Kikuta, T.; Nakatani, N. Influence of Annealing on Microstructure and NO2-Sensing Properties of Sputtered WO3 Thin Films. *Sensors Actuators, B Chem.* **2007**, *128* (1), 173–178. https://doi.org/10.1016/j.snb.2007.06.001.

(34) Srivastava, V.; Jain, K. Highly Sensitive NH3 Sensor Using Pt Catalyzed Silica Coating over WO3 Thick Films. *Sensors Actuators, B Chem.* **2008**, *133* (1), 46–52. https://doi.org/10.1016/j.snb.2008.01.066.

(35) Wu, R. J.; Chang, W. C.; Tsai, K. M.; Wu, J. G. The Novel CO Sensing Material CoOOH-WO3 with Au and SWCNT Performance Enhancement. *Sensors Actuators, B Chem.* **2009**, *138* (1), 35–41. https://doi.org/10.1016/j.snb.2009.02.014.

(36) Hsu, W. C.; Chan, C. C.; Peng, C. H.; Chang, C. C. Hydrogen

Sensing Characteristics of an Electrodeposited WO3 Thin Film Gasochromic Sensor Activated by Pt Catalyst. *Thin Solid Films* **2007**, *516* (2–4), 407–411. https://doi.org/10.1016/j.tsf.2007.07.055.

(37) Ippolito, S. J.; Kandasamy, S.; Kalantar-Zadeh, K.; Wlodarski, W. Hydrogen Sensing Characteristics of WO3 Thin Film Conductometric Sensors Activated by Pt and Au Catalysts. *Sensors Actuators, B Chem.* **2005**, *108* (1-2 SPEC. ISS.), 154–158. https://doi.org/10.1016/j.snb.2004.11.092.

(38) Solis, J. L.; Saukko, S.; Kish, L.; Granqvist, C. G.; Lantto, V. Semiconductor Gas Sensors Based on Nanostructured Tungsten Oxide. *Thin Solid Films* **2001**, *391* (2), 255–260. https://doi.org/10.1016/S0040-6090(01)00991-9.

(39) Kukkola, J.; Mäklin, J.; Halonen, N.; Kyllönen, T.; Tóth, G.; Szabó, M.; Shchukarev, A.; Mikkola, J. P.; Jantunen, H.; Kordás, K. Gas Sensors Based on Anodic Tungsten Oxide. *Sensors Actuators, B Chem.* **2011**, *153* (2), 293–300. https://doi.org/10.1016/j.snb.2010.10.043.

(40) Nugroho, F. A. A.; Darmadi, I.; Cusinato, L.; Susarrey-Arce, A.; Schreuders, H.; Bannenberg, L. J.; da Silva Fanta, A. B.; Kadkhodazadeh, S.; Wagner, J. B.; Antosiewicz, T. J.; et al. Metal–Polymer Hybrid Nanomaterials for Plasmonic Ultrafast Hydrogen

Detection. *Nat. Mater.* **2019**, *18* (5), 489–495. https://doi.org/10.1038/s41563-019-0325-4.

(41) Chávez, F.; Pérez-Sánchez, G. F.; Goiz, O.; Zaca-Morán, P.; Peña-Sierra, R.; Morales-Acevedo, A.; C. Felipe; Soledad-Priego, M. Sensing Performance of Palladium-Functionalized WO 3 Nanowires by a Drop-Casting Method. *Appl. Surf. Sci.* **2013**, *275*, 28–35. https://doi.org/10.1016/j.apsusc.2013.01.145.

(42) Nikfarjam, A.; Fardindoost, S.; Zad, A. I. Fabrication of Pd Doped WO3 Nanofiber as Hydrogen Sensor. *Polymers (Basel).* **2013**, *5* (1), 45–55. https://doi.org/10.3390/polym5010045.

(43) Fardindoost, S.; Iraji zad, A.; Rahimi, F.; Ghasempour, R. Pd Doped WO 3 Films Prepared by Sol-Gel Process for Hydrogen Sensing. *Int. J. Hydrogen Energy* **2010**, *35* (2), 854–860. https://doi.org/10.1016/j.ijhydene.2009.11.033.

(44) Boudiba, A.; Zhang, C.; Umek, P.; Bittencourt, C.; Snyders, R.; Olivier, M. G.; Debliquy, M. Sensitive and Rapid Hydrogen Sensors Based on Pd-WO3 Thick Films with Different Morphologies. *Int. J. Hydrogen Energy* **2013**, *38* (5), 2565–2577. https://doi.org/10.1016/j.ijhydene.2012.11.040.

(45) Shen, Y.; Yamazaki, T.; Liu, Z.; Meng, D.; Kikuta, T.; Nakatani, N.

Influence of Effective Surface Area on Gas Sensing Properties of WO3 Sputtered Thin Films. *Thin Solid Films* **2009**, *517* (6), 2069–2072. https://doi.org/10.1016/j.tsf.2008.10.021.

(46) Calavia, R.; Mozalev, A.; Vazquez, R.; Gracia, I.; Cané, C.; Ionescu, R.; Llobet, E. Fabrication of WO3 Nanodot-Based Microsensors Highly Sensitive to Hydrogen. *Sensors Actuators, B Chem.* **2010**, *149* (2), 352–361. https://doi.org/10.1016/j.snb.2010.06.055.

(47) Boudiba, A.; Roussel, P.; Zhang, C.; Olivier, M. G.; Snyders, R.; Debliquy, M. Sensing Mechanism of Hydrogen Sensors Based on Palladium-Loaded Tungsten Oxide (Pd-WO3). *Sensors Actuators, B Chem.* **2013**, *187*, 84–93. https://doi.org/10.1016/j.snb.2012.09.063.

(48) Esfandiar, A.; Irajizad, A.; Akhavan, O.; Ghasemi, S.; Gholami, M. R. Pd-WO3/Reduced Graphene Oxide Hierarchical Nanostructures as Efficient Hydrogen Gas Sensors. *Int. J. Hydrogen Energy* **2014**, *39* (15), 8169–8179. https://doi.org/10.1016/j.ijhydene.2014.03.117.

# Abstract (in Korean)


**금속 산화물 기반 플라즈몬 가스 센서**

plasmonics 분야는 지난 수십 년 동안 많은 관심을 받았으며 다양한 응용 분야에 적용 가능성을 보여주었습니다. 다양한 응용 분야 중 특히 가스 감지를 목적으로 하는 플라즈몬 (plasmonics)에 대한 연구가 활발히 진행되고 있다. 가스 센서의 감도, 선택도 및 내구성을 향상시키기 위해 가스 센서의 광 센서로서 플라즈몬을 사용하는 것에 대한 많은 연구가 이루어졌습니다. 광학 센서는 전압을 가할 필요가 없으며 전자기적으로 노이즈에 영향을 받지 않으며 가열 메커니즘을 필요로 하지 않으므로 반도체식 센서에 비해 더 높은 신뢰도를 보인다.

본 연구에서, 플라즈몬 공명의 전자기 강화와 결합 된 광학 간섭의 개념을 기반으로 가스 검출을 위한 센서를 설계하였다. 센서의 플라즈몬 층과 빛의 상호 작용에 의해 야기 된 국부적 인 표면 플라즈몬 공명 (LSPR)과 표면 플라즈몬 분극 (SPP)은 다양한 색의 센서를 제조하는데 이용되었다. 색상은 Lumerical software Finite Difference Time Domain (FDTD) 솔루션을 통해 시뮬레이션 하였다. Reflectance 를 위해 Si 기판 위에 Al layer를 thermal evaporator로 증착 하였다. 이후 e-beam evaporator를 이용해 $WO_3$ 박막 또는 $WO_3$ nanorods 구조체를 제작하였다. 최종적으로 Au 필름을 증착하여 plasmonic 효과를 분석하였다.

센서의 플라즈몬 층에서 발생하는 공진은 환경 변화에 매우 민감하다. 따라서, 촉매로서 귀금속으로 장식 된 나노 구조 금속 산화물은 기체의 흡착 및 탈착을 위한 유전체 매체로 사용되었다. 가스의 흡착으로 인해 센서의 광학적 특성에 변화가 생길 것으로 예상하였으며, 그 결과 산란, 흡수 및 투과 스펙트럼에서 피크 시프트가 발생할 것으로 기대한다. 이러한 피크 시프트와 색 변화가 플라즈몬 센서의 가스 감지 능력을 판별하는 파라미터로 사용된다.

**키워드:** 텅스텐 옥사이드, 금속 산화물 나노 구조체, 광 센서, 국부적인 표면 플라즈몬 공명, 광학 간섭, 금속 나노 입자

**학번:** 2017-22001

**김 준 호**